Acta Crystallographica Section B
Structural Science
ISSN 0108-7681

Structural characterization of YV_4O_8: simultaneous analysis of coexisting polytypes and simulation of diffuse scattering for a stacking disorder model

Mitsuko Onoda,* Anne-Claire Dhaussy and Yasushi Kanke

Advanced Materials Laboratory, National Institute for Material Science, Namiki 1-1, Tsukuba, Ibaraki 305-0044, Japan

Correspondence e-mail: onoda.mitsuko@nims.go.jp

Received 12 December 2002
Accepted 12 May 2003

The structure of a crystal of newly synthesized YV_4O_8 was refined on the assumption that two polytypes and their respective twin forms intergrow. The model was expressed as a commensurate composite crystal with two types of subsystem: one is a V_4O_8 framework with rather large tunnels and the other consists of Y ions. In the tunnels, Y ions and vacancies are located at every second site in an ordered manner that is characteristic of each polytype. Refinement was performed using a high-dimensional formalism and all reflections from all domains. Diffuse streaks observed in the X-ray and electron diffraction patterns were simulated using the matrix method that has been used for one-dimensional disorder such as stacking faults. The unusual diffraction phenomena that occur in a crystal of YV_4O_8 are explained as arising from a multiple-domain structure of coexisting polytypes.

1. Introduction

In a previous study by our group (Kanke & Kato, 1997), the new phases α-YbV_4O_8 (low-temperature form) and β-YbV_4O_8 (high-temperature form) were synthesized by solid-state reaction. Crystal structures of the α- and β-forms were determined by X-ray diffractometry using a single crystal and a twinned one, respectively (Kanke & Kato, 1997; Kato *et al.*, 1997). The structure of the α-form was described with a monoclinic cell (1): $P12_1/n1$, $a = 9.0648\ (3)$, $b = 10.6215\ (4)$, $c = 5.7607\ (1)$ Å, $\beta = 90.184\ (3)^\circ$, $Z = 4$. The structure of the β-form was determined using a twinned specimen and described with a monoclinic cell (2): $P2_1/n11$, $a = 9.0625\ (7)$, $b = 11.0086\ (9)$, $c = 5.7655\ (5)$ Å, $\alpha = 105.07\ (7)^\circ$, $Z = 4$. For the sake of comparison between the α-form and the β-form, which has an A-centered pseudo-orthorhombic cell dimension with the relation $\mathbf{A} = \mathbf{a}$, $\mathbf{B} = 2\mathbf{b} + \mathbf{c}$, the structure of the β-form was described based on a monoclinic cell: $A2_1/d11$, $A = 9.035\ (5)$, $B = 21.44\ (3)$, $C = c = 5.752\ (2)$ Å, $\alpha = 89.911\ (3)^\circ$, $Z = 8$ (Kanke & Kato, 1997). The three-dimensional V—O frameworks of the two forms are similar to the framework of Fe—O in orthorhombic $CaFe_2O_4$ (Decker & Kasper, 1957). In α- and β-YbV_4O_8, Yb ions occupy half of the [8]-coordinated sites in the tunnel of the framework running parallel to [001] ordered in ways that are characteristic of α- and β-YbV_4O_8, resulting in two types of superstructure of the $CaFe_2O_4$ type.

Owing to the structural similarities of α- and β-YbV_4O_8, the possibility of intergrowths of the two forms was expected in the real crystals. Actually, the diffraction pattern of the crystal illustrated features that could originate from a multiple-

domain crystal (Friese *et al.*, 1997). The structure was refined as a commensurate composite crystal with two types of subsystems, a V_4O_8 part and a Yb part, using higher-dimensional formalism and the reflections of all domains simultaneously (Friese *et al.*, 1997). All reflections in the diffraction pattern can be indexed using a lattice with a = 9.057 (1), b = 21.238 (5) and c = 5.7560 (9) Å, yet multiple domains have to be taken into account to explain the diffraction pattern.

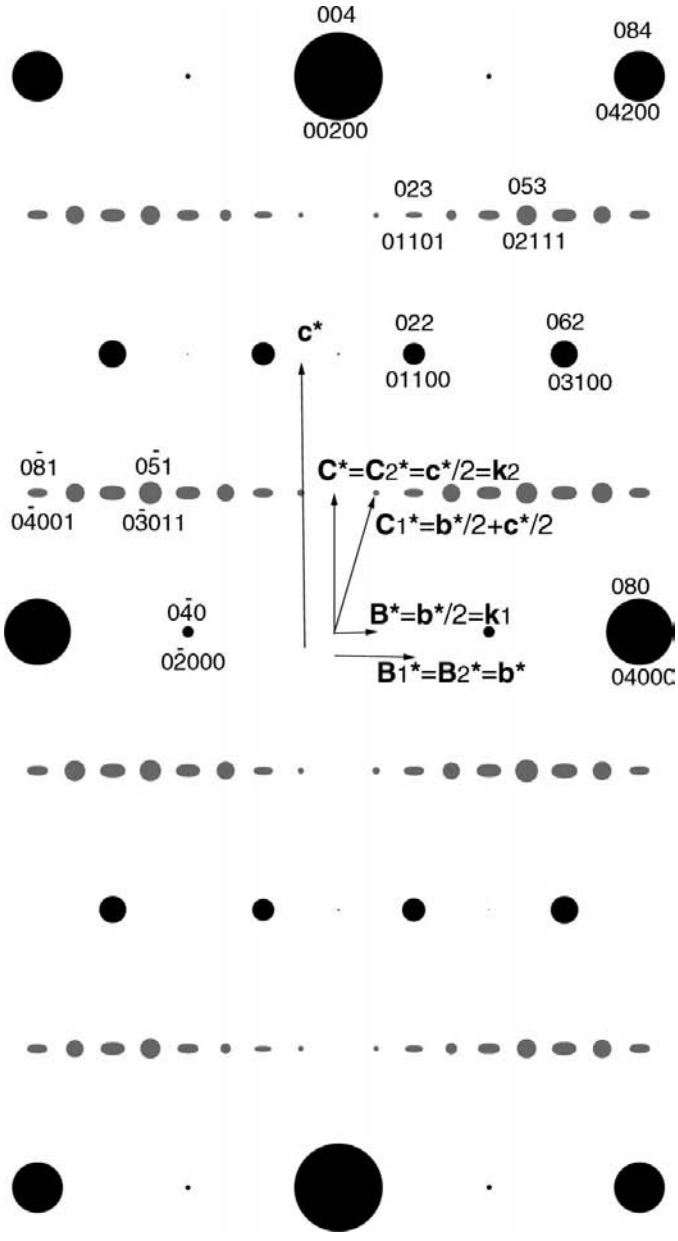

Figure 1
The measured reflections plotted schematically. Three-dimensional indices *HKL* are based on the unit cell used for data collection (A = 9.109, B = 21.356, C = 5.774 Å, $\alpha \simeq 90$, $\beta \simeq 90$, $\gamma = 90°$), while five-dimensional indices *hklmn* are based on **a**, **b**, **c**, $\mathbf{k}_1 = \mathbf{b}^*/2$, $\mathbf{k}_2 = \mathbf{c}^*/2$ (a = 9.109, b = 10.678, c = 2.887 Å, $\alpha \simeq 90$, $\beta \simeq 90$, $\gamma = 90°$). Solid circles assigned by *hkl*00 represent the main reflections common to α- and β-YV_4O_8. Hatched circles assigned by *hkl*11 represent super-reflections that originate from the β-form and they can be indexed based on A_1 = 9.109, B_1 = 11.061, C_1 = 5.774 Å, α = 105.129°. Hatched ellipses represent streaky reflections assigned by *hkl*01 that originate from the α-form and can be indexed on a pseudo-orthorhombic cell with A_2 = 9.109, B_2 = 10.678, C_2 = 5.774 Å. Relations between the reciprocal basic vectors are $\mathbf{A}^* = \mathbf{a}^* = \mathbf{A}_1^* = \mathbf{A}_2^*$, $2\mathbf{B}^* = \mathbf{b}^* = \mathbf{B}_1^* = \mathbf{B}_2^*$, $\mathbf{C}_1^* = \mathbf{b}^*/2 + \mathbf{c}^*/2$, $\mathbf{C}^* = \mathbf{c}^*/2 = \mathbf{C}_2^*$, which are equivalent for the vector relations $\mathbf{A}_1 = \mathbf{a} = \mathbf{A}_1 = \mathbf{A}_2$, $\mathbf{B}_1 = \mathbf{b} - \mathbf{c}$, $\mathbf{B} = \mathbf{b} = \mathbf{B}_2$, $\mathbf{C} = 2\mathbf{c} = \mathbf{C}_1 = \mathbf{C}_2$.

Both α- and β-YbV_4O_8 contain V^{3+}—V^{4+} mixed-valence V atoms with similar V—O frameworks. Therefore, the magnetic properties and electrical conductivities are interesting from the viewpoint of Mott's transition. However, trials to investigate the magnetic properties of α- and β-YbV_4O_8 failed (Kanke & Kato, 1997) because of the ferromagnetic pyrochlore impurity $Yb_2V_2O_7$.

In the Y—V—O system, the new phases α- and β-YV_4O_8 have been synthesized and identified to be isomorphous with α- and β-YbV_4O_8. The Y—V—O system is free from the ferromagnetic pyrochlore phase. In addition, Y^{3+} is free from f electrons. The magnetism of the α- and β-YV_4O_8 phases has been investigated and discussed.

Single crystals have been prepared near the lower limit of the existence temperature range of β-YV_4O_8 (high-temperature form). After X-ray diffraction measurements from a single crystal using an automatic diffractometer, the diffraction pattern seems to have been assigned based on a pseudo-orthorhombic unit cell with lattice constants A = 9.109, B = 21.356, C = 5.774 Å. All strong reflections could be indexed based on a pseudo-orthorhombic cell with a = 9.109, b = 10.678, c = 2.887 Å, and other weak reflections could be considered to originate from the two types of superstructure of the $CaFe_2O_4$ type: one being the α-form and the other the β-form. The crystals have been considered to be intergrowths of the two forms and are expected to be multiple-domain crystals such as YbV_4O_8 (Friese *et al.*, 1997). The Weissenberg photographs and electron diffraction patterns of the crystals, however, revealed that weak super-reflections which originate from the α-form are diffuse, while super-reflections from the β-form and all strong main reflections are sharp.

First, in the present work the structure of a multiple-domain crystal of YV_4O_8 was refined on the assumption that the α-form, the β-form and their respective twin forms intergrow. The model was expressed as a commensurate composite crystal with two types of subsystem (Janner & Janssen, 1980; Kato, 1994); one is V_4O_8 and the other is Y, and the refinement was performed using high-dimensional formalism and reflections (all) from all domains simultaneously. Next, the diffuse streaks observed in the X-ray and electron diffraction patterns were simulated using the matrix method that has been used for one-directional disorder such as stacking faults (Hendricks & Teller, 1942; Kakinoki & Komura, 1965; Kakinoki, 1967; Kato *et al.*, 1990).

2. Experimental

The starting materials V_2O_5 (99.9%) and Y_2O_3 (99.9%) were dried immediately before use at 873 and 1273 K, respectively. V_2O_3 was prepared by reducing V_2O_5 in an H_2/N_2 atmosphere at 1073 K for 2 h. V_2O_4 was obtained by heating an equimolar mixture of V_2O_5 and V_2O_3 in a sealed silica tube at 1273 K for

3 d. YVO_4 was synthesized by heating an equimolar mixture of Y_2O_3 and V_2O_5 at 1473 K for 3 d. YVO_3 was prepared by reducing YVO_4 in an H_2/N_2 atmosphere at 1273 K for 1 d.

A powder specimen of α-YV_4O_8 was prepared as follows. YVO_3, YVO_4 and V_2O_3 were mixed in a 1.1:0.9:3 molar ratio. Approximately 2 g of the mixture was placed in a platinum crucible, sealed in an evacuated silica tube and heated at 1473 K for 1 d. The product obtained was characterized to be α-YV_4O_8 by X-ray powder diffraction.

β-YV_4O_8 was prepared as follows. YVO_3, YVO_4 and V_2O_3 were mixed in a 1.1:0.9:3 molar ratio. Approximately 0.5 g of the mixture was sealed in a platinum tube and heated at 1673 K for 3 d. Both the crystalline specimen for the diffraction study and the specimen for magnetic susceptibility were obtained from the same batch.

The crystalline products of β-YV_4O_8 were investigated by Weissenberg photographs and single-crystal diffractometry. Weissenberg photographs were taken with a camera radius of 27.3 mm (Enraf–Nonius) and Ni-filtered Cu $K\alpha$ radiation. The X-ray diffraction data were collected from a single crystal with an Enraf–Nonius CAD-4 automatic diffractometer using graphite-monochromated Mo $K\alpha$ radiation (Table 1).

The remaining products of β-YV_4O_8 were crushed and characterized by X-ray powder diffraction and electron diffraction. Electron diffraction patterns were taken using a 100 kV electron microscope (JEOL-1010).

The magnetic susceptibilities of α- and β-YV_4O_8 were obtained using a SQUID magnetometer (Quantum Design).

3. Results

3.1. Symmetry consideration

Part of the measured diffraction pattern is illustrated schematically in Fig. 1. The observed 3546 reflections [$I > 2\sigma(I)$] seem to be of three groups: the first indexed based on a pseudo-orthorhombic cell with a = 9.109, b = 10.678, c = 2.887 Å, $\alpha \simeq 90$, $\beta \simeq 90$, $\gamma = 90°$, the second group indexed on a monoclinic cell with A_1 = 9.109, B_1 = 11.061, C_1 = 5.774 Å, α = 105.129°, and the third group indexed on a pseudo-orthorhombic cell with A_2 = 9.109, B_2 = 10.678, C_2 = 5.774 Å. Relations between the basic vectors are $\mathbf{A}_1 = \mathbf{A}_2 = \mathbf{a}$, $\mathbf{B}_1 = \mathbf{b} -$

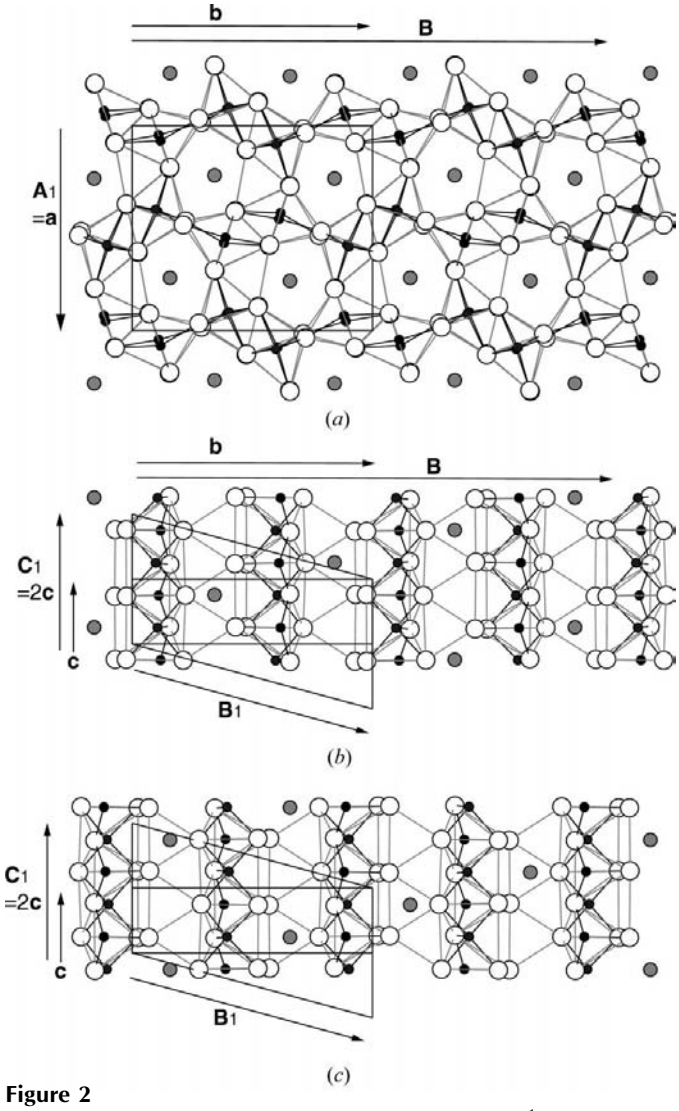

Figure 2
(*a*) Projection along $-\mathbf{C}$; (*b*) bounded projection ($0 < x < \frac{1}{2}$) along $-\mathbf{A}$; (*c*) bounded projection ($\frac{1}{2} < x < 1$) along $-\mathbf{A}$ of β-YV_4O_8. Small solid, large open and medium hatched circles represent V, O and Y, respectively.

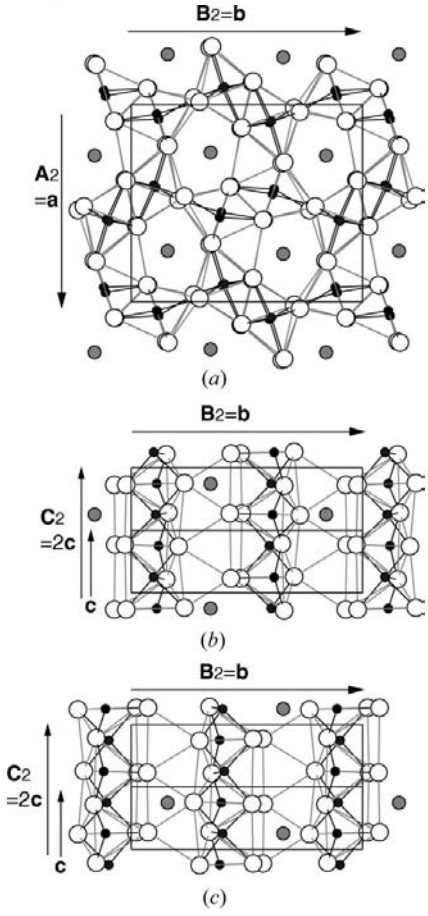

Figure 3
(*a*) Projection along $-\mathbf{C}$; (*b*) bounded projection ($0 < x < \frac{1}{2}$) along $-\mathbf{A}$; (*c*) bounded projection ($\frac{1}{2} < x < 1$) along $-\mathbf{A}$ of α-YV_4O_8. Small solid, large open and medium hatched circles represent V, O and Y, respectively.

Table 1
Experimental details.

Crystal data	
Chemical formula	YV_4O_8
M_r	420.67
Cell setting, superspace group	Monoclinic, $P2_1/n11(0\ \frac{1}{2}\ 0)(0\ 0\ \frac{1}{2})000s00$ for subsystem 1,2 $P12_1/a1(0\ 0\ \frac{1}{2})0s0$ for subsystem 3,4
a, b, c (Å)	9.109 (1), 10.687 (1), 2.887 (1)
β (°)	90
V (Å^3)	281.04 (5)
Z	2
D_x (Mg m^{-3})	4.98
Radiation type	Mo $K\alpha$
No. of reflections for cell parameters	22
θ range (°)	0–30
μ (mm^{-1})	165.13
Temperature (K)	293
Crystal form, color	Block, black
Crystal size (mm)	0.12 × 0.11 × 0.10
Data collection	
Diffractometer	Enraf–Nonius CAD4
Data collection method	ω–2θ
Absorption correction	Gaussian
T_{min}	0.1741
T_{max}	0.2795
No. of measured, independent and observed parameters	4443, 4443, 3546
Criterion for observed reflections	$I > 2\sigma(I)$
R_{int}	0.040
θ_{max} (°)	30.0
Range of h, k, l	$-12 \Rightarrow h \Rightarrow 12$ $-30 \Rightarrow k \Rightarrow 30$ $0 \Rightarrow l \Rightarrow 7$
No. and frequency of standard reflections	3 every 240 min
Intensity decay (%)	0
Refinement	
Refinement on	F
$R[F^2 > 2\sigma(F^2)]$, $wR(F^2)$	0.046, 0.055,
$hkl00$ common main (α- and β-forms)	0.037, 0.050 (1615 reflections)
$hkl11$ super-reflections (β-form)	0.052, 0.065 (1461 reflections)
$hkl01$ super-reflections (α-form)	0.108, 0.129 (470 reflections)
No. of reflections	3546
No. of parameters	97
No. of structural parameters	92
No. of scale factors	4
No. of parameters for extinction correction	1
H-atom treatment	No H atoms present
Weighting scheme	Calculated $w = 1$
Temperature factor	Anisotropic (Y and V of β-type) and isotropic (O of β-type and Y, V and O of α-type)
$(\Delta/\sigma)_{max}$	<0.0001

Computer programs: *FMLSM* (Kato, 1994).

Table 2
Minimum system, $\boldsymbol{\sigma}$, $\mathbf{Z}$ matrices, symmetry and twin operations.

$\mathbf{M}^*$	$\mathbf{a}^*, \mathbf{b}^*, \mathbf{c}^*$ (a = 9.109, b = 10.678, c = 2.887 Å)
$\boldsymbol{\sigma}$ matrix	$(0\ \frac{1}{2}\ 0 \mid 0\ 0\ \frac{1}{2})$
$\mathbf{Z}$ matrix of subsystem	$Z^1 = (1\ 0\ 0\ 0\ 0 \mid 0\ 1\ 0\ 0\ 0 \mid 0\ 0\ 1\ 0\ 0)$
	$Z^2 = (1\ 0\ 0\ 0\ 0 \mid 0\ 1\ 0\ 0\ 0 \mid 0\ 0\ 0\ 1\ 1)$
	$Z^3 = (1\ 0\ 0\ 0\ 0 \mid 0\ 1\ 0\ 0\ 0 \mid 0\ 0\ 1\ 0\ 0)$
	$Z^4 = (1\ 0\ 0\ 0\ 0 \mid 0\ 1\ 0\ 0\ 0 \mid 0\ 0\ 0\ 0\ 1)$
Symmetry operations	(i) x, y, z, u, v
	(ii) $-x, -y, -z, -u, -v$
	(iii) $\frac{1}{2}-x, \frac{1}{2}+y, \frac{1}{2}+z, u, \frac{1}{2}+v$
	(iv) $\frac{1}{2}+x, \frac{1}{2}-y, \frac{1}{2}-z, -u, \frac{1}{2}-v$
	(v) x, y, z, u, v
	(vi) $-x, -y, -z, -u, -v$
	(vii) $\frac{1}{2}+x, \frac{1}{2}-y, z, -u, \frac{1}{2}+v$
	(viii) $\frac{1}{2}-x, \frac{1}{2}+y, -z, u, \frac{1}{2}-v$
Domain 1	Subsystem 1(V, O), 2(Y)
	Symmetry operation 1–4
	Atoms 1–7 for β-YV_4O_8
Domain 2	Subsystem 1(V, O), 2(Y)
	(Twin operation $x, -y, z, -v, w$) × (symmetry operation 1–4)
	Atoms 1–7 for β-YV_4O_8
Domain 3	Subsystem 3(V, O), 4(Y)
	Symmetry operation 5–8
	Atoms 8–14 for α-YV_4O_8
Domain 4	Subsystem 3(V, O), 4(Y)
	(Twin operation $x, y, -z, u, -v$) × (symmetry operation 5–8)
	Atom 8–14 for α-YV_4O_8

$\mathbf{c}$, $\mathbf{B}_2 = \mathbf{b}$, $\mathbf{C}_1 = \mathbf{C}_2 = 2\mathbf{c}$, which are equivalent to the relations between the reciprocal vectors $\mathbf{A}_1^* = \mathbf{A}_2^* = \mathbf{a}^*$, $\mathbf{B}_1^* = \mathbf{B}_2^* = \mathbf{b}^*$, $\mathbf{C}_1^* = \mathbf{b}^*/2 + \mathbf{c}^*/2$, $\mathbf{C}_2^* = \mathbf{c}^*/2$. If we adopt five reciprocal basic vectors, $\mathbf{a}^*$, $\mathbf{b}^*$, $\mathbf{c}^*$, $\mathbf{k}_1 = \mathbf{b}^*/2$, $\mathbf{k}_2 = \mathbf{c}^*/2$, each reflection is expressed by $\mathbf{q} = h\mathbf{a}^* + k\mathbf{b}^* + l\mathbf{c}^* + m\mathbf{k}_1 + n\mathbf{k}_2$. The first group (1615 reflections) is assigned by $hkl00$ and is considered to be the main group of reflections common to α- and β-YV_4O_8. The second group (1461 reflections) assigned by $hkl11$ are super-reflections that originate from the β-form, while the third group (470 reflections) assigned by $hkl01$ are super-reflections that originate from the α-form. After consulting the results of the structural characterization of YbV_4O_8 (Kanke & Kato, 1997; Kato *et al.*, 1997; Friese *et al.*, 1997), structure models of α- and β-YV_4O_8 are expressed as commensurate composite crystals consisting of basically common V_4O_8 frameworks and different arrangements of Y ions and vacancies in the tunnels of the framework.

Reciprocal basic vectors of the two subsystems of β-YV_4O_8, ($\mathbf{a}^*, \mathbf{b}^*, \mathbf{c}^*$) for the V_4O_8 part and ($\mathbf{a}^*, \mathbf{b}^*, \mathbf{C}_1^* = \mathbf{k}_1 + \mathbf{k}_2$) for the Y part, are related to a five-dimensional basis ($\mathbf{a}^*, \mathbf{b}^*, \mathbf{c}^*, \mathbf{k}_1, \mathbf{k}_2$) through $Z^1 = (1\ 0\ 0\ 0\ 0 \mid 0\ 1\ 0\ 0\ 0 \mid 0\ 0\ 1\ 0\ 0)$ and $Z^2 = (1\ 0\ 0\ 0\ 0 \mid 0\ 1\ 0\ 0\ 0 \mid 0\ 0\ 0\ 1\ 1)$. Symmetry operations are expressed in a five-dimensional formalism based on ($\mathbf{a}^*, \mathbf{b}^*, \mathbf{c}^*, \mathbf{k}_1, \mathbf{k}_2$): x, y, z, u, v; $-x, -y, -z, -u, -v$; $\frac{1}{2}-x, \frac{1}{2}+y, \frac{1}{2}+z, u, \frac{1}{2}+v$; $\frac{1}{2}+x, \frac{1}{2}-y, \frac{1}{2}-z, -u, \frac{1}{2}-v$. This implies systematic reflection conditions; no conditions for $hklmn$, $k + l + n$ = even for $0klmn$ and h = even for $h0000$. Observed reflections with $k + l + n$ = odd for $0klmn$ in Fig. 1 are considered to originate from the (010) twinning of the β-form. Reciprocal basic vectors of the two subsystems of α-YV_4O_8, ($\mathbf{a}^*, \mathbf{b}^*, \mathbf{c}^*$) for the V_4O_8 part and ($\mathbf{a}^*, \mathbf{b}^*, \mathbf{C}_2^* = \mathbf{k}_2$) for the Y part, are related to the basis ($\mathbf{a}^*, \mathbf{b}^*, \mathbf{c}^*, \mathbf{k}_1, \mathbf{k}_2$) through $Z^3 = (1\ 0\ 0\ 0\ 0 \mid 0\ 1\ 0\ 0\ 0 \mid 0\ 0\ 1\ 0\ 0)$ and $Z^4 = (1\ 0\ 0\ 0\ 0 \mid 0\ 1\ 0\ 0\ 0 \mid 0\ 0\ 0\ 0\ 1)$. Symmetry operations for the model are expressed in a five-dimensional formalism based on the basis ($\mathbf{a}^*, \mathbf{b}^*, \mathbf{c}^*, \mathbf{k}_1, \mathbf{k}_2$): x, y, z, u, v; $-x, -y, -z, -u, -v$; $\frac{1}{2}+x, \frac{1}{2}-y, z, u, \frac{1}{2}+v$; $\frac{1}{2}-x, \frac{1}{2}+y, -z, -u, \frac{1}{2}-v$, and they

Table 3
Atomic parameters of β-YV_4O_8 and α-YV_4O_8.

In the row for Y, atomic parameters with s.u.'s are listed based on $A_1 = 9.109$, $B_1 = 11.061$, $C_1 = 5.774$ Å, $\alpha = 105.129°$ for β-YV_4O_8 and based on $A_2 = 9.109$, $B_2 = 10.678$, $C_2 = 5.774$ Å, $\beta = 90°$ for α-YV_4O_8. In the first rows for V and O, fundamental parameters with s.u.'s are listed based on a, b and c for both β-YV_4O_8 and α-YV_4O_8. In the second rows for V and O, the cosine amplitudes with s.u.'s of the Fourier series of the modulation function for the wavevector $\mathbf{k}_1 + \mathbf{k}_2$ (= $\mathbf{b}^*/2 + \mathbf{c}^*/2$) in subsystem 1 or $\mathbf{k}_2$ (= $\mathbf{c}^*/2$) in subsystem 3 are listed based on $a = 9.109$, $b = 10.678$, $c = 2.887$ Å, $\alpha = \beta = \gamma = 90°$.

No.	Atom	Subsystem	x	y	z	$100U\|U_{eq}$ (Å^2)
Domains I and II (β-YV_4O_8)						
1	Y	2	0.24249 (7)	0.34248 (5)	0.5505 (2)	1.16 (2)
2	V1	1	0.05925 (8)	0.11438 (6)	0.75	0.51 (2)
			0.0154 (1)	0.00378 (9)	0.0017 (4)	0.01 (2)
3	V2	1	0.41425 (6)	0.10157 (5)	0.25	0.41 (2)
			0.0092 (2)	0.0084 (2)	0.0029 (8)	−0.02 (5)
4	O1	1	0.2059 (2)	0.1561 (2)	0.25	0.36(6)
			0.007 (1)	−0.003 (1)	0.074 (4)	0.0
5	O2	1	0.1165 (3)	0.4756 (2)	0.25	0.39 (6)
			−0.0033 (6)	0.0008 (5)	−0.022 (2)	0.0
6	O3	1	0.4742 (3)	0.2171 (2)	0.75	0.44 (6)
			0.0099 (4)	−0.0050 (4)	−0.001 (1)	0.0
7	O4	1	0.4168 (2)	0.4289 (2)	0.25	0.29 (5)
			0.0027 (8)	−0.0024 (6)	−0.026 (2)	0.0
Domains III and IV (α-YV_4O_8)						
8	Y	4	0.24249	0.34248	0.8730 (5)	0.29 (6)
9	V1	3	0.05925	0.11438	0.75	0.3 (1)
			−0.0185 (8)	−0.0053 (5)	−0.003 (2)	0.1 (1)
10	V2	3	0.41425	0.10157	0.25	0.5 (2)
			−0.0057 (8)	−0.0060 (6)	0.000 (2)	0.0 (1)
11	O1	3	0.2059	0.156	0.25	2.2 (4)
			−0.004 (3)	−0.007 (3)	−0.049 (9)	0.0
12	O2	3	0.1165	0.4756	0.25	2.2
			0.003 (4)	−0.004 (3)	−0.03 (1)	0.0
13	O3	3	0.4742	0.2171	0.75	2.2
			−0.014 (4)	0.018 (4)	0.01 (1)	0.0
14	O4	3	0.4168	0.4289	0.25	2.2
			−0.001 (4)	0.003 (3)	−0.03 (1)	0.0

imply systematic reflection conditions; no conditions for $hklmn$, $h + n$ = even for $h0l0n$ and k = even for $0k0m0$.

3.2. Structure refinement

Simultaneous refinement of the α- and β-forms is attempted, because no pure single crystal of either the α- or β-form has been obtained. The diffuse reflections along $\mathbf{b}^*$ probably originate from the somewhat defective stacking along $\mathbf{b}$ of the α-type order arrangement of Y along $\mathbf{c}$. The number of reflections from the α-form is considerable and the reflections are expected to bring about fairly good results, although diffuseness can affect the precision of the atomic parameters of the α-form.

The reflections violating the reflection conditions of the β-form suggest (010) twinning of the β-form. Although no reflection violates the reflection conditions of the α-form, preliminary refinement using the (001) twin model of the α-form has improved convergence. Then, the two twin domains for the α- and β-forms have been considered. The twin operations for the α- and β-forms are x, y, z, u, v; $x, -y, z, -u, v$ and x, y, z, u, v; $x, y, -z, u, -v$, respectively. Relations among reciprocal bases, $\boldsymbol{\sigma}$, $\mathbf{Z}$, symmetry operations and twin operations are shown together in Table 2. The three-dimensional atomic arrangement is related to a five-dimensional structure factor with the help of the matrix $\mathbf{P}^{-1}$ derived from the $\mathbf{Z}$ and σ matrixes (Kato, 1990).

Refinement was performed on the basis of $|F|$ through the program *FMLSM* (Kato, 1994) with unit weight for all reflections. All 3546 intensity data [$I > 2\sigma(I)$] of the three groups were used after re-indexing based on ($\mathbf{a}^*$, $\mathbf{b}^*$, $\mathbf{c}^*$, $\mathbf{k}_1$, $\mathbf{k}_2$), namely 1615 reflections of (hkl00), 1461 reflections of (hkl11) and 470 reflections of (hkl01). In the structure-factor calculation a summation over two points along [00011] or [00001] can be used rather than integration.

Structures of α- and β-YV_4O_8 are described as commensurate composite crystals. Composite crystals consist of two interpenetrating substructures. In the β-form, Y ions occupy every second [8]-coordinated site along [001] in the tunnels of the V_4O_8 framework and the unit cell of the Y part is $\mathbf{A}_1 = \mathbf{a}$, $\mathbf{B}_1 = \mathbf{b} - \mathbf{c}$, $\mathbf{C}_1 = 2\mathbf{c}$. Its cell volume is twice the basic cell volume of the V_4O_8 part based on $\mathbf{a}$, $\mathbf{b}$, $\mathbf{c}$, and no modulation of Y occurs from the influence of V_4O_8. On the other hand, modulations of V and O occur through the influence of Y and vacancies in the tunnels. In the α-form, the Y ions and vacancies are arranged regularly with a unit cell $\mathbf{A}_2 = \mathbf{a}$, $\mathbf{B}_2 = \mathbf{b}$, $C_2 = 2\mathbf{c}$ and with double the cell volume of the V_4O_8 part. No modulation of Y occurs, while V and O are modulated through the influence of Y and vacancies, just like in the β-form.

For Y, the atomic coordinates and thermal parameters, anisotropic in the β-form and isotropic in the α-form, were adopted as structural parameters. The accuracy of the α-form parameters is estimated to be lower than that of the β-form parameters because of the small volume ratio of the α- to the β-form and probably weakened super-reflection intensities of the α-form owing to diffuseness. Besides, the basic atomic coordinates of V and O that are common to the α- and β-forms, the cosine amplitudes for the wavevector $\mathbf{k}_1 + \mathbf{k}_2$ (= $\mathbf{b}^*/2 + \mathbf{c}^*/2$) in the β-form or $\mathbf{k}_2$ (= $\mathbf{c}^*/2$) in the α-form were adopted as variable parameters and the sine terms were fixed to be zero after considering the structural degree of freedom of the β- and α-forms. The thermal parameters adopted are anisotropic modulated for the V atoms of the β-form, isotropic modulated for the V atoms of the α-form, isotropic individual

Table 4
Selected interatomic distances (Å).

β-YV_4O_8					
Y—O1	2.465 (4)	V1—O1	2.077 (4)	V2—O1	1.991 (4)
Y—O1^{i}	2.427 (4)	V1—O1^{i}	2.062 (4)	V2—O2^{viii}	2.007 (4)
Y—O2	2.306 (4)	V1—O3^{ii}	1.970 (5)	V2—O2^{iii}	1.988 (4)
Y—O2^{i}	2.302 (4)	V1—O4^{iii}	1.986 (4)	V2—O2^{ix}	2.016 (4)
Y—O3	2.395 (4)	V1—O4^{iv}	1.944 (4)	V2—O3^{x}	1.940 (4)
Y—O3^{ii}	2.425 (4)	V1—O4^{ii}	1.928 (4)	V2—O3	1.952 (4)
Y—O4	2.324 (4)	V1^{i}—O1^{i}	1.967 (4)	V2^{i}—O1^{i}	1.982 (4)
Y—O4^{i}	2.301 (4)	V1^{i}—O1^{v}	1.979 (4)	V2—O2^{iii}	1.983 (4)
		V1^{i}—O3^{vi}	1.976 (5)	V2—O2^{vii}	2.000 (4)
		V1^{i}—O4^{vii}	1.928 (4)	V2—O2^{ii}	2.021 (4)
		V1^{i}—O4^{ii}	2.052 (4)	V2—O3	2.017 (4)
		V1^{i}—O4^{v}	2.071 (4)	V2—O3^{i}	2.008 (4)
α-YV_4O_8					
Y—O1^{i}	2.37 (3)	V1—O1	1.99 (2)	V2—O1	1.98 (2)
Y—O1^{v}	2.48 (2)	V1—O1^{i}	1.99 (2)	V2—O2^{xvi}	2.03 (2)
Y—O2^{i}	2.32 (2)	V1—O3^{xii}	1.90 (3)	V2—O2^{xvii}	1.98 (2)
Y—O2^{v}	2.27 (2)	V1—O4^{xii}	2.03 (3)	V2—O2^{xiii}	2.03 (2)
Y—O3^{i}	2.35 (3)	V1—O4^{xi}	2.05 (2)	V2—O3^{x}	2.06 (3)
Y—O3^{xi}	2.40 (3)	V1—O4^{xiii}	2.00 (2)	V2—O3	1.94 (3)
Y—O4^{i}	2.29 (2)	V1^{i}—O1^{i}	2.07 (2)	V2^{i}—O1^{i}	2.00 (2)
Y—O4^{v}	2.31 (3)	V1^{i}—O1^{v}	2.013 (2)	V2^{i}—O2^{xviii}	2.01 (2)
		V1^{i}—O3^{xi}	2.06 (3)	V2^{i}—O2^{xiii}	2.01 (2)
		V1^{i}—O4^{xi}	1.96 (3)	V2^{i}—O2^{xv}	1.96 (2)
		V1^{i}—O4^{xiv}	1.96 (2)	V2^{i}—O3	1.90 (2)
		V1^{i}—O4^{xv}	1.99 (2)	V2^{i}—O3^{i}	2.02 (3)

Symmetry codes based on **a**, **b** and **c**: (i) $x, y, z+1$; (ii) $x-\frac{1}{2}, \frac{1}{2}-y, \frac{3}{2}-z$; (iii) $\frac{1}{2}-x, y-\frac{1}{2}, \frac{1}{2}+z$; (iv) $x-\frac{1}{2}, \frac{1}{2}-y, \frac{1}{2}-z$; (v) $x, y, z+2$; (vi) $x-\frac{1}{2}, \frac{1}{2}-y, \frac{5}{2}-z$; (vii) $\frac{1}{2}-x, y-\frac{1}{2}, \frac{3}{2}+z$; (viii) $\frac{1}{2}-x, y-\frac{1}{2}, z-\frac{1}{2}$; (ix) $\frac{1}{2}+x, \frac{1}{2}-y, \frac{1}{2}-z$; (x) $x, y, z-1$; (xi) $x-\frac{1}{2}, \frac{1}{2}-y, z+1$; (xii) $x-\frac{1}{2}, \frac{1}{2}-y, z$; (xiii) $\frac{1}{2}-x, y-\frac{1}{2}, 1-z$; (xiv) $x-\frac{1}{2}, \frac{1}{2}-y, z+2$; (xv) $\frac{1}{2}-x, y-\frac{1}{2}, 2-z$; (xvi) $\frac{1}{2}+x, \frac{1}{2}-y, z$; (xvii) $\frac{1}{2}-x, y-\frac{1}{2}, -z$; (xviii) $\frac{1}{2}+x, \frac{1}{2}-y, z+1$.

for the O atoms of the β-form and isotropic common for the O atoms of the α-form.

Furthermore, four scale factors and one parameter for the extinction correction were considered as parameters. The agreement[1] was satisfactory with 92 structural parameters; $R_F = 0.046$ and $wR_F = 0.055$. The final parameters are listed in Table 3. The structure models of the α- and β-forms are illustrated using the program *PRJMS* (Yamamoto, 1993) in Figs. 2 and 3 based on the final parameters. The final *F*-based scale factors are 0.673 (2), 0.659 (2), 0.231 (4) and 0.277 (4), and they correspond to the volume ratio of twin domains I, II, III, IV 8.48 (5):8.13 (5):1.00:1.44 (7), as the volume of each domain is proportional to the square of the scale factor. Domains I and II correspond to two twin domains of β-YV_4O_8 while domain III and IV are two twin domains of α-YV_4O_8. The parameter for extinction correction is $1.12\,(4) \times 10^{-5}$. The R_F and wR_F values for the three reflection data groups, the superposition of the common main reflections *hkl*00, super-reflections *hkl*11 from domains I and II, and super-reflections *hkl*01 from domains III and IV are listed in Table 1. Selected interatomic distances are listed in Table 4.

[1] Supplementary data for this paper are available from the IUCr electronic archives (Reference: CK0019). Services for accessing these data are described at the back of the journal.

3.3. X-ray diffraction pattern in Weissenberg photographs and electron diffraction patterns

In a Weissenberg photograph of the *HK*1 layer based on the cell used for data collection, streaks along **B*** are present at $K = 2n$ and sharp reflections are at $K = 2n + 1$. In the electron diffraction patterns with incident beams perpendicular to **B***, namely parallel to **A**, **A** + **C** and **A** + 2**C**, streaks and sharp reflections also appear alternately along **B*** at $K = 2n$ and $K = 2n + 1$. The pattern with the incident beam parallel to the *A* axis is shown in Fig. 4. As the positions of the streaks are regarded as those of the super-reflections of α-YV_4O_8, we considered that the microdomains of the α-form were brought about because of positional disorder of columns in which Y sites and vacancies alternate along **c**.

3.4. Simulation of diffuse scattering intensities

The diffuse intensity distributions may be examined on the basis of the stacking disorder model. The multiple-domain structure including microdomains of the α-form can be described in terms of the stacking sequence along the *b* direction of the elementary slice units whose sizes are expressed by a, $b' = b/2$, $c' = 2c$. Two elementary slice units, the *P* and *Q* units, are shown in Fig. 5. They are respectively derived from the atomic coordinates of the α-form between $0 < y < \frac{1}{2}$ and $\frac{1}{2} < y < 1$, based on **a**, **b**, 2**c**, and local symmetries within the slice units are x, y, z and $x+\frac{1}{2}, 1-y, \frac{1}{2}+z$, based

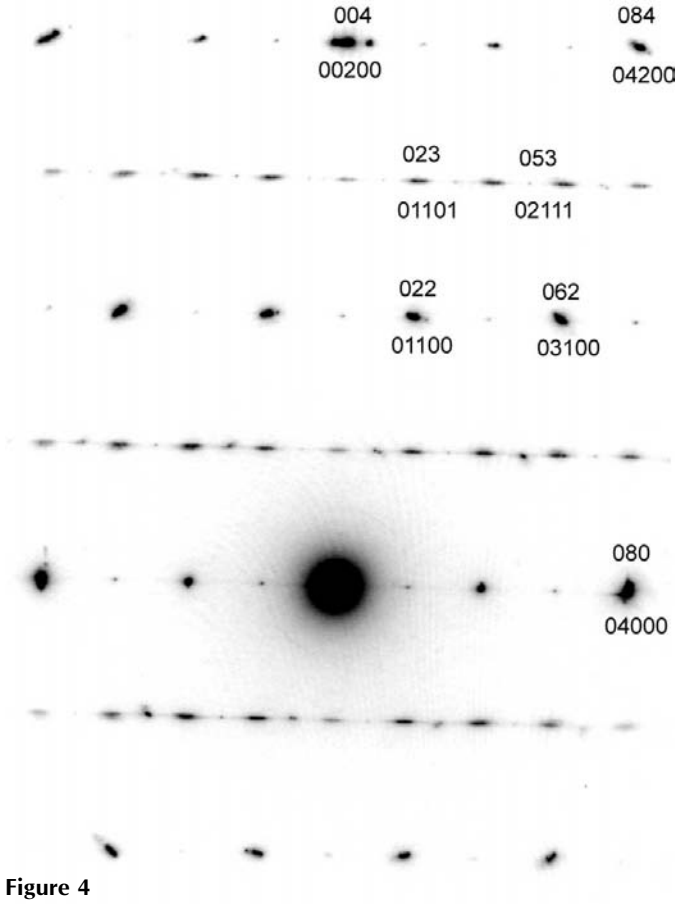

Figure 4
Electron diffraction pattern from YV_4O_8.

on **a**, **b**′ = **b**/2 **c**′ = 2**c**. The intensity was calculated using the matrix method, taking into account a probability matrix **P** for the stacking sequence, where $(\mathbf{P})_{st} = P_{st}$ and P_{st} is the probability of finding the tth stacking mode after the sth stacking mode. If the tth stacking mode is P or Q, the stacking sequence could be expressed by selecting a unit, a P or Q unit, over the last unit after shifting by a vector **b**′. We use the other stacking mode P_s or Q_s, which indicates a selection of P or Q units over the last unit with a shift vector of **b**′ + **c**′/2. The models of the α-form and its twin structure are expressed by $PQPQ\ldots$ and $Q_sP_sQ_sP_s\ldots$, while those of the β-form and its twin structure are expressed by $P_sQP_sQ\ldots$ and $PQ_sPQ_s\ldots$. After some trials, the model of Table 5 was expected to approximate the actual structure. The P-type stacking sequences are divided into three types: P^1, P^2 and P^3. P^1 and P^2 (or P^3) are distinguished from each other by the type of preceding stacking, namely Q or Q_s. P^2 and P^3 are distinguishable by the type of second former stacking, namely P or P_s. In the same manner, Q, P_s and Q_s are divided into their respective three groups. In the model, P^1, Q^1, P_s^1 and Q_s^1 are followed respectively by Q, P, Q_s and $P_s$with probability $1-\gamma$, and followed respectively by Q_s, P_s, Q and P with probability γ. P^2, Q^2, P_s^2 and Q_s^2 are resectively followed by Q_s, P_s, Q and P with probability $1-\delta$, and followed by Q, P, Q_s and P_s with probability δ. P^3, Q^3, P_s^3 and Q_s^3 are respectively followed by Q_s, P_s, Q and P with probability $1-\varepsilon$, and followed by Q, P, Q_s and P_s with probability ε. P^1, Q^1, P_s^1 and Q_s^1 constitute α-type sequences, while P^2, Q^2, P_s^2 and Q_s^2 constitute β-type sequences after repeating twice or more, P^3, Q^3, P_s^3 and Q_s^3 are β-type sequences appearing just after α-type sequences. The intensity calculation was performed with the program *FU*1 (Kato *et al.*, 1990), which has been applied to solve the structure of $Pb_{0.333}V_2O_5$. The results of the intensity calculation using the parameter values $\delta = 0.01$ and $\gamma = \varepsilon = 0.15$ are shown in Fig. 6 for the reciprocal coordinates $0\eta'L$ with L = 0, 1, 2, 3 and 4 based on **a**, **b**′ = **b**/2, **c**′ = 2**c**.

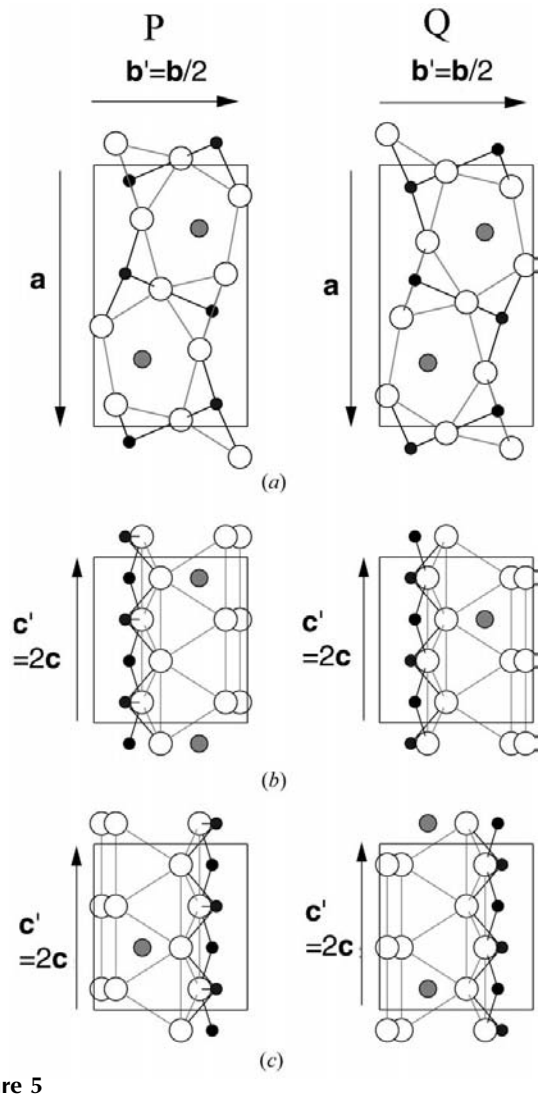

Figure 5
Elementary slice units P and Q. (*a*) Projection along $-\mathbf{c}'$; (*b*) bounded projection ($0 < x < \frac{1}{2}$) along $-\mathbf{a}$; (*c*) bounded projection ($\frac{1}{2} < x < 1$) along $-\mathbf{a}$.

3.5. Magnetic susceptibility

Fig. 7(*a*) shows the magnetic susceptibility, χ, of α-YV_4O_8. Above 78 K, χ can be expressed as the sum of the Curie–Weiss term and a temperature-independent term (Table 6). The Curie constants obtained correspond to intermediates between 4 ($S = 1/2$) per formula unit and 3 ($S = 1/2 + S = 1$) per formula unit. Negative Weiss temperatures indicate antiferromagnetic interactions. At 78 K, χ shows a small jump and increases linearly with decreasing temperature. Then, χ shows a maximum at 52 K (external field H = 0.1 T) or 51 K (H = 5.0 T) and decreases abruptly. About 60–70% of χ vanishes on the transition. For H = 0.1 T, χ increases again below 25 K and exhibits an antiferromagnetic behavior at 12 K. For H = 0.5 T, on the other hand, χ is almost constant down to 5 K.

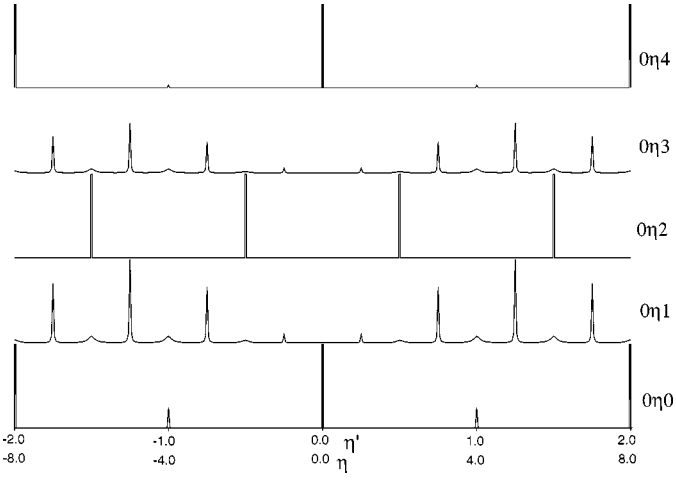

Figure 6
Intensity distributions of X-ray diffuse scattering corresponding to $0\eta'L$ with L = 0, 1, 2, 3 and 4, calculated for the model of Table 5. Reciprocal coordinates η' and indices H, L are based on **a**, **b**′ = **b**/2, **c**′ = 2**c**. Reciprocal coordinates based on **A** = **a**, **B** = 2**b**, **C** = 2**c** can be represented as $0\eta L$ and they are to be compared with the three-dimensional indices HKL of Figs. 1 and 4.

Table 5
Probability table (**P** table) for a model.

Stacking mode	Elementary unit	Shift vector
P	P	$\mathbf{b}'$
Q	Q	$\mathbf{b}'$
P_s	P	$\mathbf{b}' + \mathbf{c}'/2$
Q_s	Q	$\mathbf{b}' + \mathbf{c}'/2$

			$l-1$		P	P_s		Q	Q_s		P_s	P		Q_s	Q
			l	Q	Q_s	Q_s	P	P_s	P_s	Q_s	Q	Q	P_s	P	P
			$l+1$	P^1	P^2	P^3	Q^1	Q^2	Q^3	P_s^1	P_s^2	P_s^3	Q_s^1	Q_s^2	Q_s^3
$l-2$	$l-1$	l													
	Q	P^1		0	0	0	$1-\gamma$	0	0	0	0	0	0	0	γ
P	Q_s	P^2		0	0	0	δ	0	0	0	0	0	0	$1-\delta$	0
P_s	Q_s	P^3		0	0	0	$1-\varepsilon$	0	0	0	0	0	0	ε	0
	P	Q^1		$1-\gamma$	0	0	0	0	0	0	0	γ	0	0	0
Q	P_s	Q^2		δ	0	0	0	0	0	0	$1-\delta$	0	0	0	0
Q_s	P_s	Q^3		$1-\varepsilon$	0	0	0	0	0	0	ε	0	0	0	0
	Q_s	P_s^1		0	0	0	0	0	γ	0	0	0	$1-\gamma$	0	0
P_s	Q	P_s^2		0	0	0	0	$1-\delta$	0	0	0	0	δ	0	0
P	Q	P_s^3		0	0	0	0	ε	0	0	0	0	$1-\varepsilon$	0	0
	P_s	Q_s^1		0	0	γ	0	0	0	$1-\gamma$	0	0	0	0	0
Q_s	P	Q_s^2		0	$1-\delta$	0	0	0	0	δ	0	0	0	0	0
Q	P	Q_s^3		0	ε	0	0	0	0	$1-\varepsilon$	0	0	0	0	0

Table 6
Curie constant, C, Weiss temperature, θ, and temperature-independent susceptibility, χ_0, of α- and β-YV_4O_8.

Upper: α-YV_4O_8, above 78 K, H = 0.1 T; middle: α-YV_4O_8, above 78 K, H = 5.0 T; lower: β-YV_4O_8, above 190 K, H = 1.0 T.

C (e.m.u. K mol^{-1})	θ (K)	χ_0 (e.m.u. mol^{-1})
1.90 (3)	−60 (2)	1.55 (6) × 10^{-3}
1.79 (3)	−54 (2)	1.53 (6) × 10^{-3}
1.44 (13)	−88 (15)	1.5 (2) × 10^{-3}

Fig. 7(*b*) shows χ for β-YV_4O_8. Above 190 K, χ can be expressed as the sum of the Curie–Weiss term and a temperature-independent term (Table 6). The Curie constant obtained corresponds to 4 (S = 1/2) per formula unit. χ shows two maxima at 190 and 83 K. Below 83 K, χ decreased abruptly, but more moderately than that of α-YV_4O_8. χ increases again below 35 K.

4. Discussion

4.1. Description of the structure

Figs. 2 and 3 show the crystal structure models of α- and β-YV_4O_8. Both structures can be regarded as superstructures of orthorhombic $CaFe_2O_4$. Fe—O and V—O frameworks are essentially the same in $CaFe_2O_4$, α-YV_4O_8 and β-YV_4O_8, and they all have rather large tunnels. The three structures are distinguished from each other by the arrangement of the cations in the tunnels. In $CaFe_2O_4$, the Ca ions occupy all available [8]-coordinated sites, while, in α- and β-YV_4O_8, the Y ions are located at every second site so that occupied and vacant sites alternate along [001]. In other words, α-YV_4O_8 and β-YV_4O_8 are composed of a V_4O_8 framework and columns of Y ions and vacancies whose repeating unit is twice the fundamental c of the framework, as in α-YbV_4O_8 or β-YbV_4O_8. The models of α- and β-YV_4O_8 could be expressed as commensurate composite crystals, as shown in Tables 2 and 3. The diffraction pattern of a crystal showed features that could originate from a fourfold domain crystal: two domains of β-YV_4O_8, domain I–II, and two domains of α-YV_4O_8, domain III–IV. After refinement of the four-domain structure, the volume ratio of the four domains are obtained as 8.48 (5):8.13 (5):1.00:1.44 (7), *i.e.* the estimated volume percentages of β- and α-YV_4O_8 are 87.2 and 12.8%. The volumes of domains III and IV, however, may be underestimated because the reflection characteristics of α-YV_4O_8 are rather diffuse.

4.2. The disordered structure of YV_4O_8

The intensity distribution of scattering was calculated based on the matrix method using the values of $\gamma = \varepsilon = 0.15$ and $\delta = 0.01$ in the model of Table 5. The distribution is shown in Fig. 6 for reciprocal coordinates $0\eta L$ based on $\mathbf{A} = \mathbf{a}$, $\mathbf{B} = 2\mathbf{b} = 4\mathbf{b}'$, $\mathbf{C} = 2\mathbf{c}$. The curves are to be compared with patterns in Figs. 1 and 4. The intensity distribution for $L = 2n$, which results in sharp and strong Bragg reflections, corresponds to the superposition of the contributions of the V_4O_8 framework, the average structure of the Y ion and vacancy columns with the fundamental period **c** of both β-YV_4O_8 and α-YV_4O_8. Simulation for $L = 2n + 1$ corresponds to the order and disorder arrangement of the Y ion and vacancy columns. Streaks pass through the positions expressed by $L = 2n + 1$ and they reflect the 2**c** repeating unit of the columns in which Y-occupied and vacant sites alternate along [001]. The diffuse maxima appear at $\eta' = -2.0, -1.5, -1.0, \ldots$ or $\eta = -8.0, -6.0, -4.0, \ldots$ and they coincide in position with those of the observed patterns. The maxima could also be indexed on a pseudo-orthorhombic cell with A_2 = 9.109, B_2 = 10.678, C_2 = 5.774 Å. The sharp

maxima on $0\eta L$ for $L = 2n + 1$ appear at $\eta' = -1.75, -1.25, -0.75, \ldots$ or $\eta = -7.0, -5.0, -3.0, \ldots$ and they coincide in position with sharp spots that could be indexed on a monoclinic cell with $A_1 = 9.109$, $B_1 = 11.061$, $C_1 = 5.774$ Å, $\alpha = 105.129^\circ$. As simulation has resulted in a good visual agreement between calculated intensities and observed patterns, the model of Table 5 is considered to give an approximate but satisfactory explanation of the streaks observed in the pattern of the multiple-domain structure of YV_4O_8.

The model means that P^2, Q^2, P_s^2 and Q_s^2, which are β-type sequences after repeating twice or more, are followed by a β-type sequence with probability 0.99 and by an α-type sequence with probability 0.01. Other sequences, namely the α-type sequence and the first β-type sequence after α-type sequences, are followed by α-type sequences with probability 0.85 and by β-type sequences with probability 0.15. In order to obtain the microscopic image of stacking sequences from the parameters, γ, δ and ε, the simulation has been attempted using random numbers and the program *SQ*3 (Kato *et al.*, 1990). Part of the model obtained for the case of $\gamma = \varepsilon = 0.15$ and $\delta = 0.01$ is illustrated in Fig. 8. Once a domain of β-YV_4O_8 has appeared, β-type sequences continue with the large probability $1 - \delta$ and the average size of the β-YV_4O_8 domain, which is rather large. On the contrary, α-type sequences are obstructed by a β-type sequence with the considerable probability γ and the average domain sizes of α-YV_4O_8 are rather small. After the β-type sequence which obstructs α-type sequences, the α-type sequence follows with large probability $1 - \varepsilon$ and the frequency of appearance of the α-YV_4O_8 domain is rather large. A single β-type sequence plays the role of a boundary between two domains of α-YV_4O_8.

The program *FU*1 could estimate the existence probability of 12 types of stacking modes, P^1, P^2, P^3, Q^1, Q^2, Q^3, ..., as 0.0735, 0.1654, 0.011, 0.0735, 0.1654, 0.011, ... As the volume ratio of domain III or IV to domain I or II is estimated as $[0.0735 \times \gamma + 0.1654 \times (1 - \delta) + 0.011 \times \varepsilon]/[0.0735 \times (1 - \gamma) + 0.1654 \times \delta + 0.011 \times (1 - \varepsilon)]$, the volume proportions 29 and 71% can be attributed to α-YV_4O_8 and β-YV_4O_8.

The crystal seems to consist of two wide domains I and II of β-YV_4O_8 and two narrow domains III and VI of α-YV_4O_8. These phase-separation-like phenomena could be the result of fluctuations in experimental conditions and/or metastable equilibrium conditions connected with the kinetics of the solid-state phase transition.

4.3. Estimation of average domain size

All diffuse streaks are centered at the positions of the α-type superstructure reflections and they indicate the presence of narrow lamellar domains of α-YV_4O_8. All β-type superstructure reflections are rather sharp and they indicate the presence of wide domains of β-YV_4O_8. We consider relations between the size distribution of domains and the continuing probabilities used in simulation of diffuse scattering intensities and then we estimate the average domain sizes of the α- and β-forms.

We denote a linear domain size, parallel to **b**, and the average linear domain size of an α-form domain, respectively, by L and R taken in the unit of $b' = b/2 = 5.339$ Å.

$$R = \sum_{L=1}^{\infty} Lq(L),$$

where $q(L)$ is a relative occurrence frequency of a domain with size L. $q(L)$ for the α-form is expected to be proportional to $(1 - \gamma)^L$, because α-type sequences are obstructed by β-type sequences with the probability γ in domains III and IV. As the summation of $(1 - \gamma)^L$, for $L = 1, 2, 3, \ldots, \infty$, is reduced to $(1 - \gamma)/\gamma$, $q(L)$ can be expressed as $(1 - \gamma)^L \times \gamma/(1 - \gamma)$. Then

$$R = \sum_{L=1}^{\infty} Lq(L) = \gamma/(1-\gamma) \times \sum_{L=1}^{\infty} L(1-\gamma)^L = \gamma/(1-\gamma) \times (1-\gamma)/\gamma^2 = 1/\gamma.$$

The average domain size of α-YV_4O_8 is expected to be the reciprocal of the disorder probability γ. In the same manner, the average domain size of β-YV_4O_8 is expected to be $1/\delta$, where $(1 - \delta)$ is the continuing probability of the β-type sequence in domains I and II.

The model of Table 5 with $\gamma = \varepsilon = 0.15$ and $\delta = 0.01$ gave a satisfactory explanation of the observed diffuse scattering. The expected average domain sizes of the α- and β-types are estimated to be $1/\gamma = 6.7$ and $1/\delta = 100$, respectively, taken in

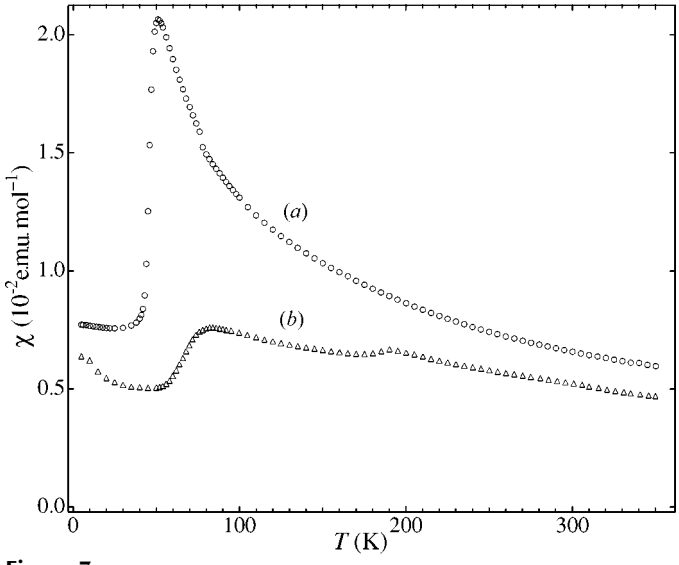

Figure 7
Temperature dependence of the magnetic susceptibility χ of (*a*) α-YbV_4O_8 and (*b*) β-YV_4O_8.

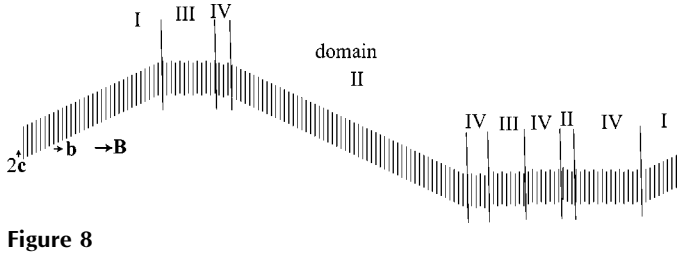

Figure 8
Schematic representation of the multiple-domain structure of YV_4O_8.

the unit of 5.339 Å. The estimated average domain sizes, ~40 Å for α-YV_4O_8 and ~500 Å for β-YV_4O_8, correspond to the model illustrated in Fig. 8, although only a limited area of sequences is illustrated in the figure.

4.4. Susceptibility and domain structures

The magnetic susceptibility χ (Fig. 7*a*) of a powder specimen of α-YV_4O_8 is considered to be intrinsic to α-YV_4O_8. On the other hand, the χ value (Fig. 7*b*) of β-YV_4O_8 obtained from the same batch as that for the diffraction study is not intrinsic to β-YV_4O_8 because the specimen consists of both α- and β-type domains. However, the latter data do not show the sharp peak at 51–52 K observed in the former data, but alternatively show a broad maximum at 83 K. One possible explanation for this fact would be the domain size effect. According to the model (Table 5, Fig. 8) and the estimated average domain size of α-YV_4O_8 (~40 Å), the broadening and peak shift in the susceptibility can be understood as resulting from the domain structure of the α-form with a small average domain size and dense domain boundaries (Fig. 8). On the other hand, the estimated average domain size of β-YV_4O_8 (~500 Å) is too large to cause the domain size effect. The rather sharp peak around 190 K in Fig. 7(*b*) is considered to be intrinsic to β-YV_4O_8 and free from the domain size effect.

5. Conclusions

Unusual diffraction phenomena observed in YV_4O_8 were examined using a commensurate composite crystal model and one-directional disorder model. The structure was refined successfully on the assumption that two different superstructures, α-YV_4O_8 and β-YV_4O_8, and their respective twin forms coexist in the crystals. Diffuse streaks centered at the positions of the α-type superspots were simulated using the matrix method for one-directional disorder and the average domain size of α-YV_4O_8 has been estimated. It has been demonstrated that the diffraction patterns arise from twin domains with the average domain size ~40 Å of α-YV_4O_8 and twin domains with large domain sizes of β-YV_4O_8.

The authors are grateful to Dr K. Kato for stimulating discussions and valuable advise.

References

Decker, B. F. & Kasper, J. S. (1957). *Acta Cryst.* **10**, 332–337.
Friese, K., Jarchow, O., Kato, K. & Kanke, Y. (1997). *Z. Kristallogr.* **212**, 859–863.
Hendricks, S. & Teller, E. (1942). *J. Chem. Phys.* **10**, 147–167.
Janner, A. & Janssen, T. (1980). *Acta Cryst.* A**36**, 408–415.
Kakinoki, J. (1967). *Acta Cryst.* **23**, 875–885.
Kakinoki, J. & Komura, Y. (1965). *Acta Cryst.* **19**, 137–147.
Kanke, K. & Kato, K. (1997). *Chem. Mater.* **9**, 141–147.
Kato, K. (1990). *Acta Cryst.* B**46**, 39–44.
Kato, K. (1994). *Acta Cryst.* A**50**, 351–357.
Kato, K., Kanke, Y. & Friese, K. (1997). *Z. Kristallogr.* **212**, 110–114.
Kato, K., Kosuda, K., Koga, T. & Nagasawa, H. (1990). *Acta Cryst.* C**46**, 1587–1590.
Yamamoto, A. (1993). *Acta Cryst.* A**49**, 831–846.